In Situ Study of Lithiation and Delithiation of MoS2 Nanosheets using Electrochemical Liquid Cell TEM

ARTICLE *in* NANO LETTERS · JULY 2015

Impact Factor: 13.59 · DOI: 10.1021/acs.nanolett.5b02483 · Source: PubMed

NANO LETTERS

Letter

pubs.acs.org/NanoLett

In Situ Study of Lithiation and Delithiation of MoS_2 Nanosheets Using Electrochemical Liquid Cell Transmission Electron Microscopy

Zhiyuan Zeng,[†] Xiaowei Zhang,[†,§] Karen Bustillo,[‡] Kaiyang Niu,[†,⊥] Christoph Gammer,[‡,⊥] Jun Xu,[§] and Haimei Zheng*[,†,⊥]

[†]Materials Sciences Division and [‡]National Center for Electron Microscopy, Molecular Foundry, Lawrence Berkeley National Laboratory, Berkeley, California 94720, United States

[§]National Laboratory of Solid State Microstructures, School of Electronic Science and Engineering and Collaborative Innovation Centre of Advanced Microstructures, Nanjing University, Nanjing 210093, China

[⊥]Department of Materials Science and Engineering, University of California, Berkeley, California 94720, United States

Supporting Information

ABSTRACT: We report the observation of lithiation/delithiation of MoS_2 nanosheets in a $LiPF_6$/EC/DEC commercial electrolyte for the application of lithium-ion batteries using electrochemical liquid cell transmission electron microscopy (TEM). Upon discharge in a voltage range of 1.8−1.2 V, MoS_2 on the Ti electrode underwent irreversible decomposition resulting in fragmentation of the MoS_2 nanosheets into 5−10 nm MoS_2 nanoparticles. Repeated experiments also show that some MoS_2 nanosheets do not decompose upon lithiation. Instead, lithiation induced structural expansion and deformation has been observed. A solid−electrolyte interface (SEI) was formed on the anode side of the Ti electrode in contact with Li metal. The SEI layer is composed of LiF nanocrystals distributed within the entire layer with the constituent elements C, O, and F. However, no passivation film was observed on the cathode side of the Ti electrode with MoS_2 nanosheets on it. Such an in situ electrochemical liquid cell TEM study sheds light on battery degradation mechanisms.

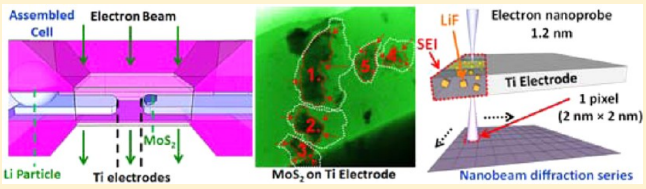

KEYWORDS: *Liquid cell TEM, electrochemical liquid cell, solid electrolyte interface, MoS_2, lithium-ion batteries*

Layered MoS_2 is an attractive electrode material for lithium-ion batteries.[1,2] For example, MoS_2 can be used as an anode material with high theoretical capacity of 1290 mAh g^{-1}.[3] Compared to other anode materials, such as silicon,[4−8] germanium,[9] or nickel oxides,[10] MoS_2 has less volume expansion[1] (103% as compared with silicon, which has a volume change of 400% upon insertion and extraction of lithium[8]), and consequently lower rates of cycling induced degradation are possible. However, when lithium ions are inserted between the layers of MoS_2, the MoS_2 structure can be exfoliated using ultrasonication treatment of lithiated MoS_2 in H_2O.[11,12] In addition, electrochemical degradation may be induced by the active material loss when MoS_2 is used as the cathode material.[13] In situ observation of lithiation and delithiation of MoS_2 as the electrode material provides critical insight regarding the degradation mechanisms of this material for battery applications.

In situ liquid cell transmission electron microscopy (TEM) has enabled imaging of chemical reactions in liquids with high spatial resolution.[14−17] This technique has facilitated the opportunity to address important questions related to the electrode−electrolyte interfaces in lithium-ion batteries in a number of studies.[18−23] For example, the lithiation and delithiation of fully submerged Si nanowire electrodes during electrochemical testing has been demonstrated using an electrochemical liquid cell TEM.[18] It has also been reported, using an in situ graphene liquid cell TEM, that the first lithiation of Si nanoparticle leads to anisotropic volume expansion favoring the ⟨110⟩ directions, followed by isotropic expansion.[19] The preferential volume expansion and fracture are also confirmed by ex situ scanning electron microscopy (SEM) characterization using crystalline Si nanopillars as the investigating object.[4,5] Lithium insertion and extraction dynamics and the degradation of $LiFePO_4$ have been observed using a combination of liquid cell TEM imaging, spectroscopy, and theoretical calculations,[20] which are very useful supplementary findings to atomic imaging of lithium staging in partially delithiated $LiFePO_4$[24] and random solid solution zone in $LiFePO_4$ electrode.[25] Other studies include the breakdown of a range of inorganic/salt complexes relevant to the state-of-the-art Li-ion battery systems by in situ scanning TEM (STEM)[21] and the formation of a solid−electrolyte interface (SEI) on graphite and gold using a standard battery electrolyte in a liquid cell under TEM.[22,23] Recently, with our newly designed electrochemical liquid TEM cells, images of the inhomogeneous lithiation of a Au electrode, dynamic dendritic growth of

Received: April 14, 2015
Revised: June 28, 2015

DOI: 10.1021/acs.nanolett.5b02483
Nano Lett. XXXX, XXX, XXX−XXX

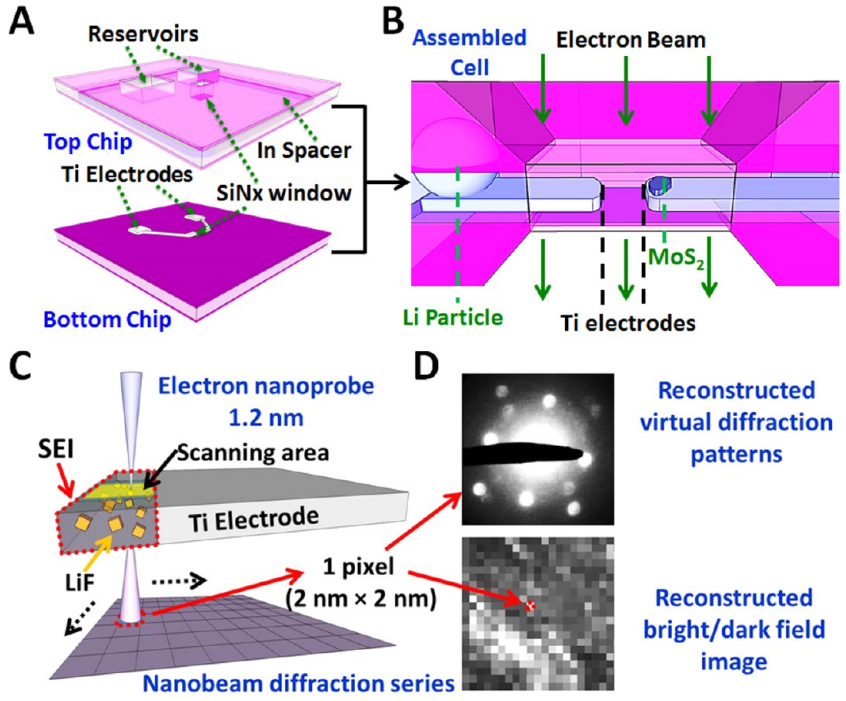

Figure 1. A schematic of the in situ TEM observation of MoS_2 reaction on Ti electrode by using an electrochemical liquid cell. (A) A top microchip patterned with 150 nm thick indium is bonded with the bottom microchip with 90 nm thick titanium electrodes to form a liquid cell for TEM visualization using a homemade TEM holder. (B) The window area in an electrochemical liquid cell shows MoS_2 nanosheets were loaded on the right side Ti electrode, and Li metal was loaded on the left side Ti electrode. The dynamic lithiation/delithiation reaction of MoS_2 nanosheets was captured as the electron beam passed through the SiNx window under TEM. (C) A schematic showing nanobeam diffraction characterization of SEI layer or residual MoS_2 products after the reaction. (D) An example of the reconstructed bright-field image or dark-field image from a nanobeam diffraction series with each pixel corresponding to a reconstructed virtual diffraction pattern.

lithium metal, electrolyte decomposition, and SEI formation were captured in real time.[26,27] Despite the progress that has been made, it is still a great challenge to study real battery systems using in situ liquid cell TEM.

Here we report the study of MoS_2 structures using a modified design of electrochemical liquid cell for TEM. We use Ti electrodes instead of Au to avoid electrode reaction with the electrolyte ($LiPF_6$/EC/DEC). It is also noted that we reduce the Ti electrode thickness from previous 120 to 90 nm to improve the imaging resolution of the active material on the electrode. Additionally, Ti metal has much lower atomic number than Au metal, which further benefits the image resolution. Most importantly, Li metal particles are loaded on one side of the electrode, which acts as both counter electrode and reference electrode. With MoS_2 introduced on the other electrode, it forms a real nanobattery cell, as shown in Figure 1, panels A and B. A detailed description of the experimental process for the liquid cell preparation can be found in the Supporting Information. Such a nanobattery offers the opportunity to study the reaction mechanism of MoS_2 during battery operation while imaging with TEM. We record movies at the rate of 10−75 frames per second for the in situ experiments. Further characterization, such as elemental analysis using energy dispersive X-ray spectroscopy (EDS) and structural identification with nanobeam diffraction, is conducted after the reaction in the liquid cell is stopped. A schematic of the nanobeam diffraction technique is shown in Figure 1, panels C and D, and more details can be found in a previous publication.[28]

The successful loading of MoS_2 nanosheets on the Ti electrode was confirmed by the TEM imaging and diffraction patterns of MoS_2 in the observatory window area, as shown in Figure S1. The sequential images in Figure 2 show the morphological evolution of MoS_2 under lithiation during discharge (also see Movie S1). The corresponding applied electrical potential and measured electrical current are plotted in Figure 2, panel G. Initially, five nanosheets were located in the window area on the Ti electrode. As the voltage was ramped down to 1.8 V, some structures dissolved, and the MoS_2 particles reacted vigorously with the electrolyte. As a consequence, more than 50% of MoS_2 nanoflakes decomposed in less than 5 s upon lithiation (Figure 2D−F). This can be related to other reports on the dissolution of electrode materials and the shuttling effect of lithium polysulfide in a real battery cell.[29] The drastic loss of MoS_2 at the applied voltage of 1.2 V is highlighted in Figure 2, panel F. The change in area of the five MoS_2 nanosheets as a function of time was extracted and plotted in Figure 2, panel H. The drastic decrease of MoS_2 during 12−18 s corresponds to the dissolution of MoS_2 in a voltage range of 1.8−1.2 V.

The discharge/charge reaction can be expressed as below:[1,13,29]

$$MoS_2 + xLi^+ + xe^- \rightarrow Li_xMoS_2\ (\sim 1.1\ V\ vs\ Li/Li^+) \quad (1)$$

$$Li_xMoS_2 + (4 - x)Li^+ + (4 - x)e^- \rightarrow Mo + 2Li_2S\ (\sim 0.6\ V\ vs\ Li/Li^+) \quad (2)$$

$$Li_2S \leftrightarrow S + 2Li^+ + 2e^-\ (\sim 2.2\ V\ vs\ Li/Li^+) \quad (3)$$

To identify the reaction products, we did EDS mapping and selected area electron diffraction (SAED) of the reacted MoS_2

DOI: 10.1021/acs.nanolett.5b02483
Nano Lett. XXXX, XXX, XXX−XXX

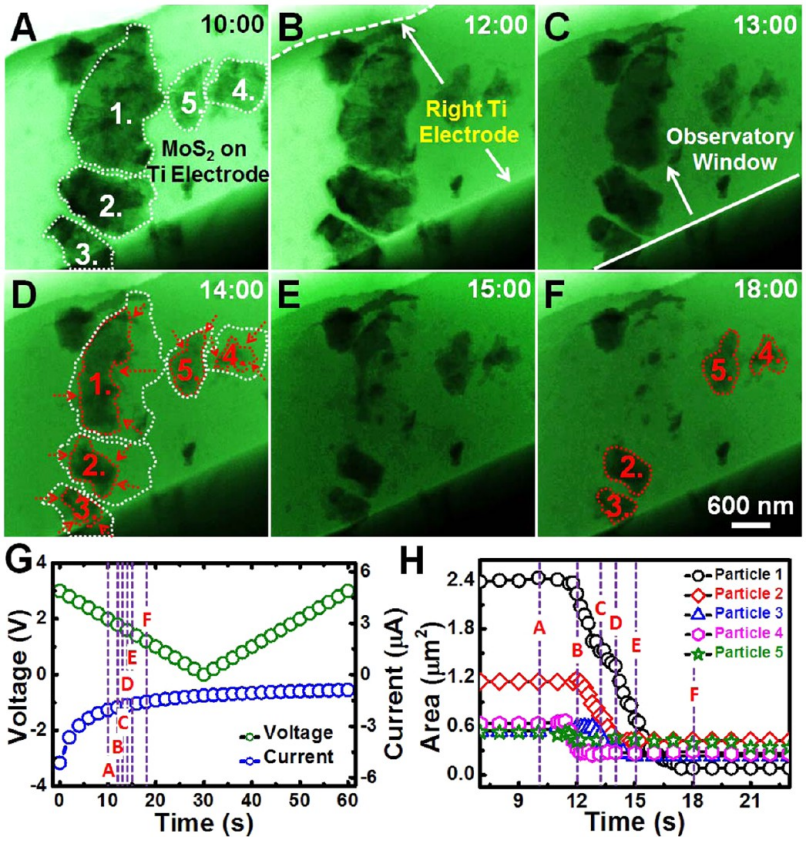

Figure 2. In situ electrochemical reaction of MoS_2 nanosheets with $LiPF_6$/EC/DEC electrolyte on the right side Ti electrode in a liquid cell. (A–F) Time series of TEM images show the morphological evolution of MoS_2 nanosheets during the first discharge of the cell. (G) The corresponding applied electric potential and measured electric current from panel A to panel F. (H) The change in area of five MoS_2 nanosheets as a function of time during cyclic voltammetry in the voltage range of 3–0 V at a scan rate of 0.1 V/s.

nanosheets on the Ti electrode. The composition of the residual lithiated MoS_2 nanosheets is confirmed by SAED patterns as shown in Figure S2B–F. High-angle annular dark-field (HAADF) imaging of the reacted MoS_2 nanosheets shows that some of the nanosheets have dissolved (Figure 3A). The EDS maps show evidence of Mo and S elements in the residual MoS_2 nanoflakes but not in the rest of areas (Figure 3B,C). It is noted that since the Mo L-series peak is overlapping with S K-series peak, we chose the Mo K-series (17.480 keV) to identify the presence of Mo and then applied the deconvoluted Mo L-series/S K-series peak to confirm the presence of sulfur. The EDS maps of F K-series and Ti K-series elements clearly show that F is homogeneously distributed in the whole observation window area, and the strong Ti signal coincides with the morphology of the Ti electrode in the HAADF image (Figure 3D,E). The EDS spectrum of reacted MoS_2 nanosheets from the dried liquid cell is shown in Figure S3. Figure 3, panel F shows the magnified HAADF image of the reacted MoS_2 nanosheet on the Ti electrode, and as marked with white dashed box in Figure 3, panel A, the white lamellar structures are residual MoS_2 nanosheets. In Figure 3, panel F, the area "G" marked with red dashed line is the region with a MoS_2 nanosheet on Ti electrode, and "H" is the region without MoS_2 nanosheet. Figure 3, panels G and H are the corresponding deconvoluted Mo L-series/S K-series spectra from the two regions after discharge. We can see that the intensity of Mo and S signals is decreased significantly in the region without MoS_2 nanosheets, which suggests that the MoS_2 nanosheets were decomposed and dissolved into the electrolyte. Although there is no obvious contrast at the regions without MoS_2 nanosheets in the HAADF STEM images, nanoparticles with diameters of 5–10 nm are visible in bright-field (BF) and low-angle annular dark-field (LAADF) using a long camera length (770 mm) in STEM to include diffraction contrast, Figure 3, panels I and J.

To identify the origin of the Mo and S signal in the region without obvious MoS_2 nanosheets, we did nanobeam diffraction in STEM mode by acquiring a series of diffraction patterns at each pixel in the scanned area. From the diffraction series (Figure 3K), we reconstructed the BF image (Figure 3L). We chose a region with 16 pixels from one of the nanoparticles marked by the red box "M" and reconstructed a virtual diffraction pattern from these pixels shown in Figure 3, panel M. The lattice spacings of 2.72 and 1.61 Å are achieved, which are assigned to {100} and {110} planes of MoS_2, respectively. Therefore, the residual nanoparticles are MoS_2. We also chose another region outside of nanoparticle, which is marked by the red box "N" and reconstructed a virtual diffraction pattern (Figure 3N). The lattice spacing of 2.33 Å was obtained, which matches Ti {110} lattice. In addition, by selecting a single diffraction spot marked in Figure 3, panels M and N, we can create virtual dark field images, as shown in Figure 3, panels O and P. It is clear that Ti electrode has a small grain size and may have polycrystalline regions, as evident from the diffraction pattern. This analysis indicates that even if the MoS_2/Li cell undergoes a deep discharge process at 0 V, the detectable residual is only MoS_2. As to why Mo or Li_2S is not detected (see eq 2 as a reference), we propose two possibilities. (1) The

DOI: 10.1021/acs.nanolett.5b02483
Nano Lett. XXXX, XXX, XXX–XXX

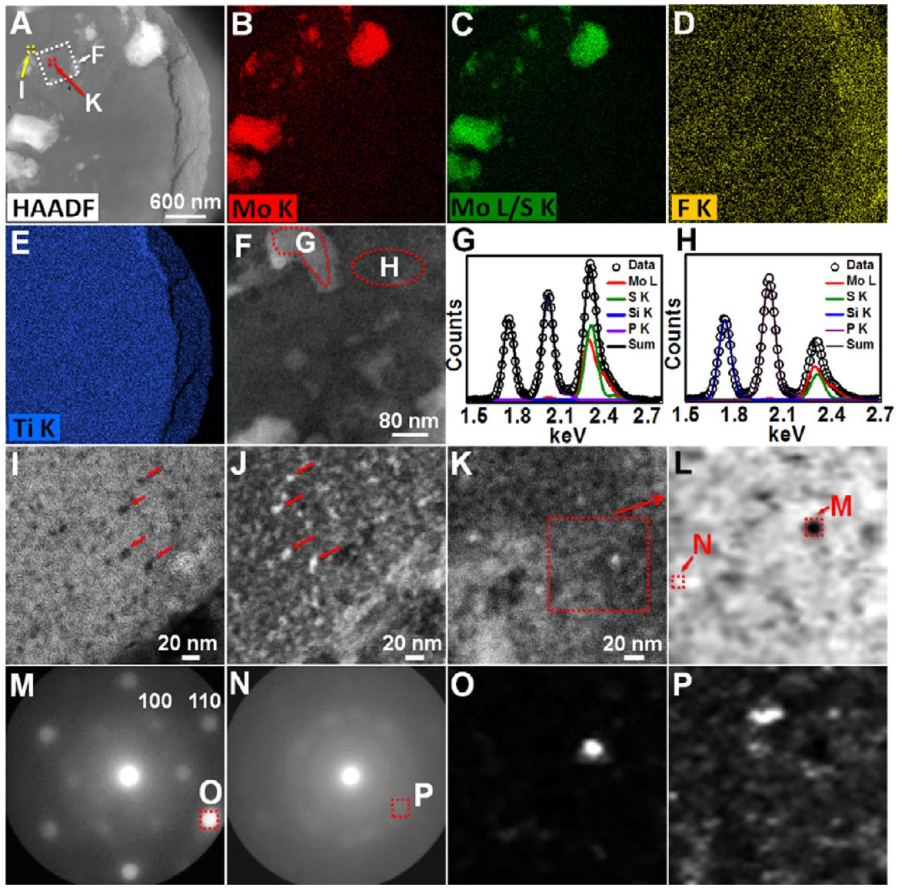

Figure 3. More detailed characterization of the residual MoS_2 on the right side Ti electrode. (A) HAADF image showing the reacted MoS_2 nanosheets and the corresponding elemental distribution from EDS mapping. (B–E) EDS maps using different elemental edges: (B) Mo K-series; (C) Mo L-series/S K-series; (D) F K-series; (E) Ti K-series. (F) Magnified HAADF image of as indicated with the white dashed box in panel A. (G) Deconvoluted spectra of Mo L-series/S K-series peak in the region with MoS_2 nanosheets and (H) a region without visible MoS_2 nanosheets. (I) BF TEM image of the residual particles on Ti electrode with particle size of 5–10 nm showing the darker contrast compared with Ti electrode background. (J) The corresponding STEM image using a long camera length (770 mm) to include diffraction contrast, and particles appear to be lighter. (K) Long camera length (770 mm) STEM image with nanobeam diffraction series acquired in the marked red dash box area. (L) The reconstructed BF image obtained from the diffraction series. (M) Reconstructed virtual diffraction patterns from the marked region with 16 pixels in panel L. (N) Reconstructed virtual diffraction patterns from the marked region with 9 pixels in panel L. (O) Virtual dark-field image reconstructed by selecting single diffraction spot marked in panel M. (P) Virtual dark-field image reconstructed by selecting single diffraction spot marked in panel N.

MoS_2 nanosheets break into small MoS_2 nanoparticles because of lithium ion intercalation induced stress during fast discharging/charging process. On the basis of the previous experimental results,[11] when the discharge cutoff voltage was set at 0.9 V (close to the discharge plateau at 1.1 V, as shown in Figure S15), the discharge reaction only proceeded to the first step, that is, $MoS_2 + xLi^+ + xe^- \rightarrow Li_xMoS_2$ (1.1 V vs Li/Li^+). After ultrasonication in deionized water, the product was exfoliated into single layers of MoS_2 nanosheets. Therefore, under the first step discharge reaction, the gap between two layers of MoS_2 has intercalated enough lithium ions to increase the layer distance and weaken the van der Waals force between the layers. It is clear that it is much easier to break a thin layer of MoS_2 into particles than bulk form of MoS_2. In this respect, the reaction of $MoS_2 + xLi^+ + xe^- \rightarrow Li_xMoS_2$ (1.1 V vs Li/Li^+) plays a critical role in the particles breaking up. (2) MoS_2 nanosheets can also decompose into amorphous Mo and Li_2S, which has been observed for a range of conversion electrodes both during lithiation and sodiation.[29−32] However, only the former scenario can be detected using nanobeam diffraction.

We found that some MoS_2 nanosheets decompose upon lithiation, while the others remain and experience structural changes, that is, swelling or deformation. The variation of the MoS_2 nanosheets during lithiation may result from the MoS_2 thickness difference or inhomogeneity during lithiation. Figure 4, panel A shows another representative structure change of MoS_2 during first discharge/charge process on the right side working electrode (also see Movie S2 and Figure S4). Upon lithiation, a reaction front is introduced, which is marked with a red arrow, as indicated in Figure 4, panel A; the reaction front propagates fast and sweeps across two large and thick MoS_2 layered nanosheets. The surrounding area of MoS_2 nanosheets becomes dark and blurry, which may result from the generation and diffusion of reaction products into the surrounding area. Eventually, the reacted areas of two MoS_2 nanosheets are merged in a cloud of reaction zone. The expansion of the MoS_2 nanosheets as a function of lithiation time has been plotted in Figure S4F. Additionally, we have also captured the dynamic movement of a wavy front of MoS_2 nanosheets in Figure 4, panel B (marked in the sequential images in Figure S5, also see Movie S3). These wavy surfaces in the reaction front indicate

DOI: 10.1021/acs.nanolett.5b02483
Nano Lett. XXXX, XXX, XXX−XXX

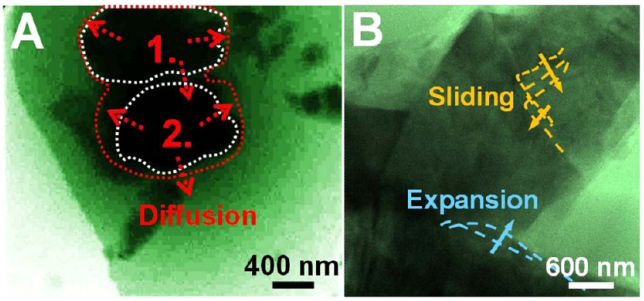

Figure 4. Other two representative structure changes of MoS_2 during first discharge/charge process on the working electrode. (A) Diffusion and (B) swelling deformation.

structural deformation during lithiation, which can result from sliding motion of slabs with respect to each other, changing of sites of the Mo atoms associated with Fermi surface nesting, and the John-Teller effect.[33−35]

In addition to the reactions of MoS_2 on the right side Ti electrode, which acts as the working electrode, we have also characterized the reactions on the left side Ti electrode, which is in contact with Li metal as the counter and reference electrode. From the extracted time series of TEM images shown in Figure 5, panels A−D (see more details in Movie S4), the thickness of SEI layer on the leading edge of the Ti electrode or MoS_2 nanosheets is observed to slowly increase as the voltage program proceeds (Figure 5F). This observation is consistent with our previous work on the lithiation of Au.[26] Figure 5, panel E is the corresponding applied electrical potential and measured electrical current from panel A to panel D. To analyze the components of SEI on the Ti electrode in contact with the Li anode, we did EDS mapping on the edge of the patterned rectangular Ti strip on the left side Ti electrode. The SEI layer has a thickness of 200 nm. The EDS maps show that besides the Ti signal from the electrode, there are signals from the elements C, O, and F in the SEI film (Figure 6B−E). In Figure 6, panel F, the EDS line scan shows raw X-ray counts from the different elements (C, O, Ti, F) as a function of distance into the SEI film on this Ti anode.

We have done further measurements to identify the composition and structure of SEI on the anode. It has been assumed that the SEI on the negative electrode of the Li-metal and Li-ion cells is composed of two distinct layers:[36−38] a compact inner layer with polycrystalline or heteromicrophase inorganic products (e.g., Li_2CO_3, LiF, Li_2O) adjacent to the electrode material, and an outer layer with porous and amorphous partially reduced organic products (e.g., $(CH_2OCO_2Li)_2$, ROLi, $ROCO_2Li$). The inner layer was expected to be at least 1.5−2 nm in thickness, and the outer layer could be on the order of 100 nm thick.[36] However, our nanobeam diffraction experiments show that the whole SEI is amorphous matrix with distributed LiF nanocrystals. Figure 6, panel G shows HAADF image of Ti electrode with SEI layer and the red dash box indicating the nanobeam scanning area of SEI. Figure 6, panel H is the reconstructed BF image originating from the acquired nanobeam diffraction series. The reconstructed diffraction patterns corresponding to the regions marked with "I" and "J" in Figure 6, panels I and J indicate the presence of LiF nanocrystals with different zone axis indexed as $[1\bar{1}0]$ and [001]. In addition, by selecting a single diffraction spot marked in Figure 6, panels I and J, we can create virtual dark-field images (Figure 6K,L), and the results confirm that the LiF nanocrystals are distributed within the whole SEI layer. It is also noted that there might be other inorganic components (e.g., Li_2CO_3, Li_2O), which could be amorphous or crystalline but not oriented in a diffracting condition, and thus would be invisible in the nanobeam diffraction experiment. It is noted that since the Ti electrode is not reactive to the $LiPF_6$/EC/DEC electrolyte, the formation of SEI should be stepwise from preferential reduction of certain electrolyte components.[39] On the contrary, the lithium metal electrode appears to react with the electrolyte, and SEI forms instantaneously. Consequently, the reduction of electrolyte components should be indiscriminate to all species.[40] The detection of protective films on the cathode surface has not been as straightforward as that of the SEI on the anode.[39] Our observation provides the direct evidence for the formation of SEI on the anode instead of the cathode, which is valuable for the understanding of the electrochemical process in general.

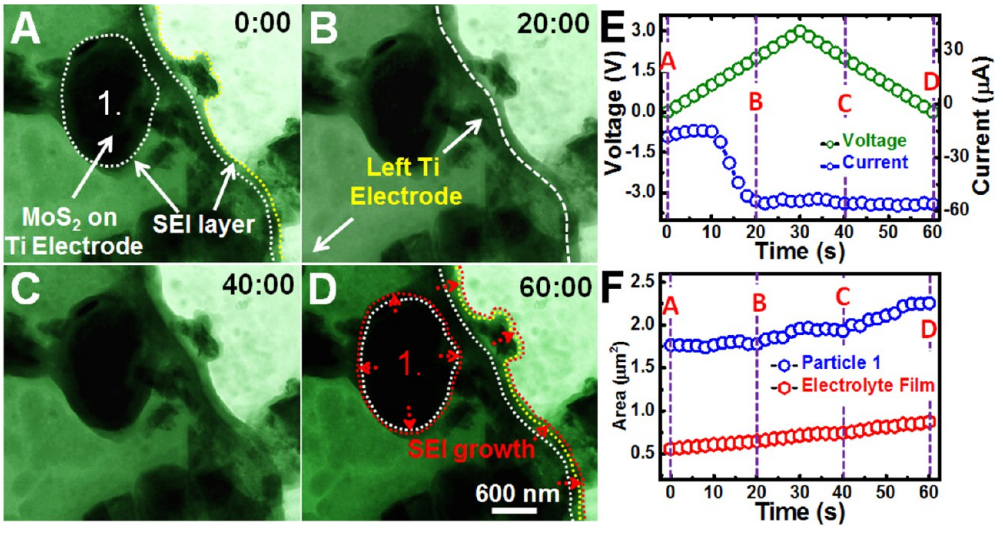

Figure 5. SEI formation on the left side Ti electrode, which is in contact with the Li metal. (A−D) Time series of TEM images showing the growth of SEI film on MoS_2 nanosheets and at the edge of the Ti electrode. (E) The corresponding applied electric potential and measured electric current from panel A to panel D. (F) Change in area of SEI layer.

DOI: 10.1021/acs.nanolett.5b02483
Nano Lett. XXXX, XXX, XXX−XXX

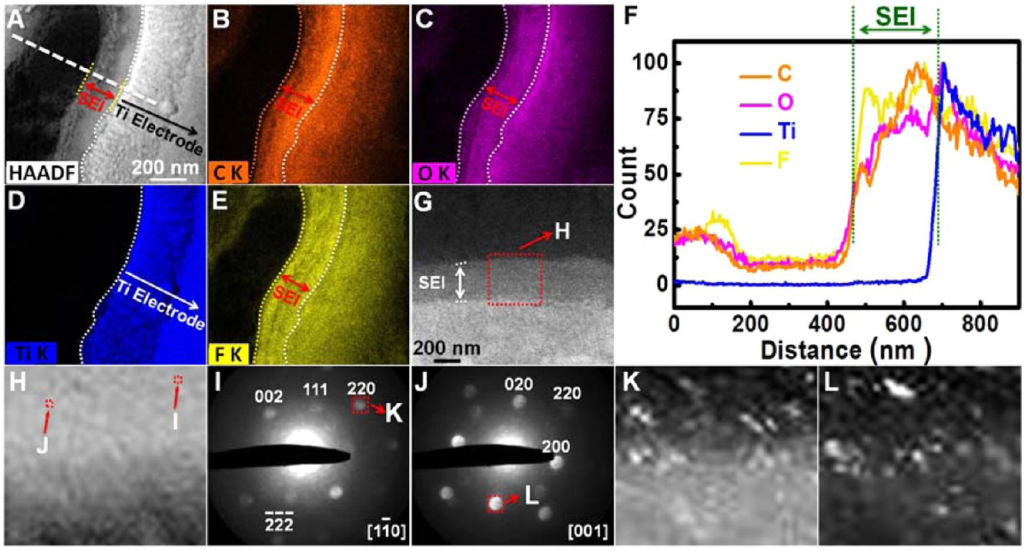

Figure 6. More detailed characterization of the SEI layer on the left side Ti electrode. (A) HAADF image of the Ti electrode with SEI film passivated on it. (B–E) The corresponding EDS maps of different elements using different EDS edges: (B) C K-series; (C) O K-series; (D) Ti K-series; (E) F K-series. (F) EDS line scan starting from SiNx membrane across the SEI layer and ending on the Ti electrode, marked in panel A. (G) HAADF image of the SEI layer formed on Ti electrode with red dash box indicating nanobeam diffraction acquiring area. (H) Reconstructed BF image obtained from the diffraction series. (I, J) Reconstructed virtual diffraction patterns selected from regions marked "I" and "J" in panel H. (K) Virtual dark-field image reconstructed using the selected single diffraction spot in panel I. (P) Virtual dark-field image reconstructed using the selected single diffraction spot in panel J.

Lastly, we note that electron beam effects are unavoidable in TEM experiments.[21,41] Nevertheless, beam damage can be minimized with reduced total electron dose during imaging. Our control experiments confirm that the irreversible decomposition of MoS_2 and dissolution of reaction products generated during lithiation reaction is not caused by e-beam. For all experiments, we make sure that without an applied cyclic voltammetry, there is no change in the MoS_2 nanosheets or other observable reactions.

In summary, we have performed a systematical study of MoS_2 lithiation reaction using electrochemical liquid cell TEM. A nanobattery cell with the commercial battery electrolyte $LiPF_6$/EC/DEC and Li metal on one electrode as counter and reference electrode was achieved. Dynamic dissolution and lithiation induced deformation of MoS_2 during charge in the voltage range of 1.8–1.2 V were captured. Irreversible decomposition near 1.1 V was observed, where MoS_2 nanosheets broke down into 5–10 nm MoS_2 nanoparticles as confirmed by nanobeam diffraction experiments. We also observed the SEI formation on the Ti anode in contact with Li metal during charge/discharge process. The composition and structure of SEI were characterized using EDS and nanobeam diffraction, which show that the SEI layer is composed of C, O, and F species with LiF nanocrystals distributed in the entire SEI layer. This in situ study of MoS_2 decomposition during lithiation in battery operation provides insights on improving the battery design and applications of transition metal dichalcogenides in related energy devices.

■ ASSOCIATED CONTENT

Supporting Information

Materials and methods. TEM images and SAED patterns of MoS_2 nanosheets loaded on Ti electrode in electrochemical liquid cell. EDS spectrum from an area with the reacted MoS_2 nanosheets on Ti electrode in electrochemical liquid cell. Time-lapse of TEM images showing the reaction and dissolution of thick MoS_2 nanoflakes on Ti electrode, and showing morphological evolution of MoS_2 nanosheets during the initial reaction with the electrolyte. Movie of lithiation of MoS_2 nanosheets under cyclic voltammetry. Movie of the reaction and dissolution of thick MoS_2 nanosheets on Ti electrode under cyclic voltammetry. Movie of the reaction and phase transition of MoS_2 nanosheets involves a slipping of slabs in the MoS_2 crystal during lithiation/delithiation. Movie of slow growth of SEI film on Ti electrode and MoS_2 nanosheets under cyclic voltammetry. The Supporting Information is available free of charge on the ACS Publications website at DOI: 10.1021/acs.nanolett.5b02483.

■ AUTHOR INFORMATION

Corresponding Author

*E-mail: hmzheng@lbl.gov.

Notes

The authors declare no competing financial interest.

■ ACKNOWLEDGMENTS

The experiments were conducted using the TEM facility JEOL2100 at Materials Sciences Division and CM 200, FEI Tecnai, and FEI Titan microscopes at the Molecular Foundry of Lawrence Berkeley National Laboratory (LBNL), which is supported by the U.S. Department of Energy (DOE) under Contract No. DE-AC02-05CH11231. X.W.Z. acknowledges the support of National Basic Research Program of China (2013CB632101) and China Scholarship Council under No. 201406190080. C.G. thanks the Austrian Science Fund (FWF): [J3397] for support. H.Z. thanks the support of DOE Office of Science Early Career Research Program and also the BEARS SinBeRise travel support. We thank Direct Electron, LP (San Diego, CA) for providing the high speed direct electron camera model DE-12 for movie capture. We acknowledge Zachary Andersen and Peter Ercius who made contribution to the

DOI: 10.1021/acs.nanolett.5b02483
Nano Lett. XXXX, XXX, XXX–XXX

development of the code used to acquire the nanobeam diffraction datasets.

REFERENCES

(1) Stephenson, T.; Li, Z.; Olsen, B.; Mitlin, D. *Energy Environ. Sci.* **2014**, *7*, 209.
(2) Radisavljevic, B.; Radenovic, A.; Brivio, J.; Giacometti, V.; Kis, A. *Nat. Nanotechnol.* **2011**, *6*, 147.
(3) Chang, K.; Chen, W. *Chem. Commun.* **2011**, *47*, 4252.
(4) Lee, S. W.; McDowell, M. T.; Choi, J. W.; Cui, Y. *Nano Lett.* **2011**, *11*, 3034.
(5) Lee, S. W.; McDowell, M. T.; Berla, L. A.; Nix, W. D.; Cui, Y. *Proc. Natl. Acad. Sci. U. S. A.* **2012**, *109*, 4080.
(6) Zeng, Z. Y.; Tu, J. P.; Yang, Y. Z.; Xiang, J. Y.; Huang, X. H.; Mao, F.; Ma, M. *Electrochim. Acta* **2008**, *53*, 2724.
(7) Zeng, Z. Y.; Tu, J. P.; Huang, X. H.; Wang, X. L.; Xiang, J. Y. *Thin Solid Films* **2009**, *517*, 4767.
(8) Chan, C. K.; Peng, H.; Liu, G.; McIlwrath, K.; Zhang, X. F.; Huggins, R. A.; Cui, Y. *Nat. Nanotechnol.* **2008**, *3*, 31.
(9) Kennedy, T.; Mullane, E.; Geaney, H.; Osiak, M.; O'Dwyer, C.; Ryan, K. M. *Nano Lett.* **2014**, *14*, 716.
(10) Lin, F.; Nordlund, D.; Weng, T.-C.; Zhu, Y.; Ban, C.; Richards, R. M.; Xin, H. L. *Nat. Commun.* **2014**, *5*, 3358.
(11) Zeng, Z.; Yin, Z.; Huang, X.; Li, H.; He, Q.; Lu, G.; Boey, F.; Zhang, H. *Angew. Chem., Int. Ed.* **2011**, *50*, 11093.
(12) Zeng, Z.; Sun, T.; Zhu, J.; Huang, X.; Yin, Z.; Lu, G.; Fan, Z.; Yan, Q.; Hng, H. H.; Zhang, H. *Angew. Chem., Int. Ed.* **2012**, *51*, 9052.
(13) Fang, X. P.; Guo, X. W.; Mao, Y.; Hua, C. X.; Shen, L. Y.; Hu, Y. S.; Wang, Z. X.; Wu, F.; Chen, L. Q. *Chem. - Asian J.* **2012**, *7*, 1013.
(14) Zheng, H.; Smith, R. K.; Jun, Y.-w.; Kisielowski, C.; Dahmen, U.; Alivisatos, A. P. *Science* **2009**, *324*, 1309.
(15) Liao, H.-G.; Cui, L.; Whitelam, S.; Zheng, H. *Science* **2012**, *336*, 1011.
(16) Liao, H.-G.; Zherebetskyy, D.; Xin, H.; Czarnik, C.; Ercius, P.; Elmlund, H.; Pan, M.; Wang, L.-W.; Zheng, H. *Science* **2014**, *345*, 916.
(17) Niu, K.-Y.; Park, J.; Zheng, H.; Alivisatos, A. P. *Nano Lett.* **2013**, *13*, 5715.
(18) Gu, M.; Parent, L. R.; Mehdi, B. L.; Unocic, R. R.; McDowell, M. T.; Sacci, R. L.; Xu, W.; Connell, J. G.; Xu, P.; Abellan, P.; Chen, X.; Zhang, Y.; Perea, D. E.; Evans, J. E.; Lauhon, L. J.; Zhang, J.-G.; Liu, J.; Browning, N. D.; Cui, Y.; Arslan, I.; Wang, C.-M. *Nano Lett.* **2013**, *13*, 6106.
(19) Yuk, J. M.; Seo, H. K.; Choi, J. W.; Lee, J. Y. *ACS Nano* **2014**, *8*, 7478.
(20) Holtz, M. E.; Yu, Y.; Gunceler, D.; Gao, J.; Sundararaman, R.; Schwarz, K. A.; Arias, T. A.; Abruña, H. D.; Muller, D. A. *Nano Lett.* **2014**, *14*, 1453.
(21) Abellan, P.; Mehdi, B. L.; Parent, L. R.; Gu, M.; Park, C.; Xu, W.; Zhang, Y.; Arslan, I.; Zhang, J.-G.; Wang, C.-M.; Evans, J. E.; Browning, N. D. *Nano Lett.* **2014**, *14*, 1293.
(22) Unocic, R. R.; Sun, X.-G.; Sacci, R. L.; Adamczyk, L. A.; Alsem, D. H.; Dai, S.; Dudney, N. J.; More, K. L. *Microsc. Microanal.* **2014**, *20*, 1029.
(23) Sacci, R. L.; Dudney, N. J.; More, K. L.; Parent, L. R.; Arslan, I.; Browning, N. D.; Unocic, R. R. *Chem. Commun.* **2014**, *50*, 2104.
(24) Gu, L.; Zhu, C. B.; Li, H.; Yu, Y.; Li, C. L.; Tsukimoto, S.; Maier, J.; Ikuhara, Y. *J. Am. Chem. Soc.* **2011**, *133*, 4661.
(25) Niu, J.; Kushima, A.; Qian, X.; Qi, L.; Xiang, K.; Chiang, Y.-M.; Li, J. *Nano Lett.* **2014**, *14*, 4005.
(26) Zeng, Z. Y.; Liang, W. I.; Liao, H. G.; Xin, H. L. L.; Chu, Y. H.; Zheng, H. M. *Nano Lett.* **2014**, *14*, 1745.
(27) Zeng, Z.; Liang, W.-I.; Chu, Y. H.; Zheng, H. *Faraday Discuss.* **2014**, *176*, 95.
(28) Gammer, C.; Burak Ozdol, V.; Liebscher, C. H.; Minor, A. M. *Ultramicroscopy* **2015**, *155*, 1.
(29) Xiao, J.; Wang, X.; Yang, X.-Q.; Xun, S.; Liu, G.; Koech, P. K.; Liu, J.; Lemmon, J. P. *Adv. Funct. Mater.* **2011**, *21*, 2840.
(30) Wang, H.; Xu, Z.; Li, Z.; Cui, K.; Ding, J.; Kohandehghan, A.; Tan, X.; Zahiri, B.; Olsen, B. C.; Holt, C. M. B.; Mitlin, D. *Nano Lett.* **2014**, *14*, 1987.
(31) Peng, C.; Chen, B.; Qin, Y.; Yang, S.; Li, C.; Zuo, Y.; Liu, S.; Yang, J. *ACS Nano* **2012**, *6*, 1074.
(32) Ding, J.; Li, Z.; Wang, H.; Cui, K.; Kohandehghan, A.; Tan, X.; Karpuzov, D.; Mitlin, D. *J. Mater. Chem. A* **2015**, *3*, 7100.
(33) Wang, L.; Xu, Z.; Wang, W.; Bai, X. *J. Am. Chem. Soc.* **2014**, *136*, 6693.
(34) Whangbo, M. H.; Canadell, E. *J. Am. Chem. Soc.* **1992**, *114*, 9587.
(35) Imanishi, N.; Toyoda, M.; Takeda, Y.; Yamamoto, O. *Solid State Ionics* **1992**, *58*, 333.
(36) Christensen, J.; Newman, J. *J. Electrochem. Soc.* **2004**, *151*, A1977.
(37) Aurbach, D.; Einely, Y.; Zaban, A. *J. Electrochem. Soc.* **1994**, *141*, L1.
(38) Bar-Tow, D.; Peled, E.; Burstein, L. *J. Electrochem. Soc.* **1999**, *146*, 824.
(39) Xu, K. *Chem. Rev.* **2004**, *104*, 4303.
(40) Peled, E. *J. Electrochem. Soc.* **1979**, *126*, 2047.
(41) Tao, R.; Todorovic, R.; Liu, J.; Meyer, R. J.; Arnold, A.; Walkosz, W.; Zapol, P.; Romanenko, A.; Cooley, L. D.; Klie, R. F. *J. Appl. Phys.* **2011**, *110*, 124313.

DOI: 10.1021/acs.nanolett.5b02483
Nano Lett. XXXX, XXX, XXX−XXX